Research Paper

μ-Opioid receptor activation modulates CA3-to-CA1 gamma oscillation phase-coupling

Yujiao Zhang[a,1], Sanya Ahmed[b,1], Georgiana Neagu[b], Yali Wang[c], Zhenyi Li[a], Jianbin Wen[c], Chunjie Liu[a], Martin Vreugdenhil[a,b,d,*]

[a] *Department of Psychology, Xinxiang Medical University, Jinsui Avenue, Xinxiang, 453003, PR China*
[b] *Department of Neuroscience, College of Medical and Dental Sciences, University of Birmingham, Vincent Drive, Birmingham, B15 2TT, United Kingdom*
[c] *Department of Neurobiology, Xinxiang Medical University, Jinsui Avenue, Xinxiang, 453003, PR China*
[d] *Department of Life Science, School of Health Sciences, Birmingham City University, Westbourne Road, Birmingham, B15 3TN, United Kingdom*

A B S T R A C T

In the intact brain, hippocampal area CA1 alternates between low-frequency gamma oscillations (γ), phase-locked to low-frequency γ in CA3, and high-frequency γ, phase-locked to γ in the medial entorhinal cortex. In hippocampal slices, γ in CA1 is phase-locked to CA3 low-frequency γ. However, when Schaffer collaterals are cut, CA1 can generate its own high-frequency γ. Here we test whether (un)coupling of CA1 γ from CA3 γ can be caused by μ-opioid receptor (MOR) modulation.

In CA1 minislices isolated from rat ventral hippocampus slices, MOR activation by DAMGO reduced the dominant frequency of intrinsic fast γ, induced by carbachol. In intact slices, DAMGO strongly reduced the dominant frequency of CA3 slow γ, but did not affect γ power consistently. DAMGO suppressed the phase coupling of CA1 γ to CA3 slow γ and increased the power of CA1 intrinsic fast γ, but not in the presence of the MOR antagonist CTAP. The benzodiazepine zolpidem and local application of DAMGO to CA3 both mimicked the reduction in dominant frequency of CA3 slow γ, but did not reduce the phase coupling. Local application of DAMGO to CA1 reduced phase coupling.

These results suggest that MOR-expressing CA1 interneurons, feed-forwardly activated by Schaffer collaterals, are responsible for the phase coupling between CA3 γ and CA1 γ. Modulating their activity may switch the CA1 network between low-frequency γ and high-frequency γ, controlling the information flow between CA1 and CA3 or medial entorhinal cortex respectively.

1. Introduction

1.1. Neuronal activity in the brain fluctuates rhythmically and synchronously

In the hippocampus, oscillations at theta frequency (θ: 3–8 Hz) and gamma frequency (γ: 30–120 Hz) are prominent during exploration (Buzsáki et al., 2003; Csicsvari et al., 2003). Hippocampal cornu ammonis area 1 (CA1) receives its major inputs from cornu ammonis area 3 (CA3) and from the medial entorhinal cortex (MEC). The 'routing by

synchrony' hypothesis proposes that information flow between areas is dynamically modulated by the level of phase-locking of the oscillations in these areas (Fries, 2009). During exploration, γ synchronization in CA1 varies in its frequency content, with low-frequency γ oscillations (slow γ: 30–60 Hz) phase-locked with slow γ in CA3, and medium-/high-frequency γ oscillations (fast γ: 60–120 Hz), prominent when CA1 receives the strongest inputs from the MEC (Montgomery and Buzsaki, 2007; Schomburg et al., 2014). Slow γ and fast γ are prominent at different phases of the θ oscillation (Colgin et al., 2009), suggesting that, timed by the θ oscillation, CA1 alternatively tunes in to CA3 and

MEC (Schomburg et al., 2014). θ coordinates the encoding and retrieval of episodic and spatial memories (Hasselmo, 2005; Jensen and Lisman, 2005). It was therefore proposed that CA3 to CA1 routing of information by phase-coupled slow γ is involved in memory retrieval, whereas MEC to CA1 information routing during fast γ is associated with encoding of new information (Belluscio et al., 2012; Bieri et al., 2014). This implies that alternating slow γ and fast γ states allows the hippocampus to switch between prospective and retrospective modes, possibly to prevent interference between memory retrieval and encoding (Colgin, 2015).

It is therefore important to understand what mechanisms underlie the switch of the CA1 network between slow γ and fast γ. Slow γ in CA1 has been shown to be driven by CA3 in vitro (Fellous and Sejnowski, 2000; Fisahn et al., 1998) and in vivo (Bragin et al., 1995), through feed-forward inhibition by parvalbumin-expressing (PV+) interneurons and bi-stratified interneurons (Bibbig et al., 2007; Tukker et al., 2007; Zemankovics et al., 2013). However, during fast γ, pyramidal CA1 firing is synchronized by local interneurons (Colgin et al., 2009; Senior et al., 2008). It was therefore proposed that "in the absence of particularly strong activation of CA3, the default gamma mode in CA1 during active behaviors may be fast gamma oscillations" (Colgin and Moser, 2010). Indeed, when disconnected from CA3, the CA1 network generates intrinsic fast γ through feedback inhibition (Bibbig et al., 2007; Middleton et al., 2008; Pietersen et al., 2014), which can be suppressed by low-intensity 33 Hz Schaffer collateral stimulation, mimicking slow γ input from CA3 (Pietersen et al., 2014).

The excitability of feed-forward interneurons may be controlled by θ phase-linked modulation (Wulff et al., 2009), possibly through activation of μ opioid receptors (MOR) expressed on PV+ interneurons (Drake and Milner, 2002; Svoboda et al., 1999) that inhibit GABAergic inhibitory postsynaptic responses in CA1 pyramidal neurons (Glickfeld et al., 2008; Lupica, 1995; Masukawa and Prince, 1982). Enkephalin release from enkephalin-expressing interneurons in area CA1 is modulated by the θ phase (Fuentealba et al., 2008b) and targets PV+ interneurons (Blasco-Ibanez et al., 1998; Fuentealba et al., 2008b), which may mediate the θ phase modulation of fast γ and slow γ in CA1. MORs are also expressed on neurogliaform and Ivy cells (Krook-Magnuson et al., 2011), but given the low frequency and slow kinetics of IPSCs elicited by these cells, their contribution to rhythm generation and exact timing of γ is limited (Armstrong et al., 2012; Price et al., 2005; Fuentealba et al., 2008a).

To investigate the role of MOR activation in the switch between fast γ and slow γ in CA1, we tested the effect of activation or inhibition of MOR in hippocampal slices.

2. Experimental procedures

2.1. Animals

Adult male Wistar rats (200–300 g) were used for in vitro experiments. All procedures conformed to the UK Animals (Scientific Procedures) Act 1986 and were approved by the Biomedical Ethics Review Sub-committee of the University of Birmingham and by the Animal ethics and administrative council of Henan province, P.R. China. All efforts were made to minimize animal suffering and to reduce the number of animals used.

2.2. Hippocampal slice preparation

Rats were anesthetized by intraperitoneal injection of a ketamine (75 mg kg^{-1})/ medetomidine (1 mg kg^{-1}) mixture and killed by cardiac perfusion with a chilled sucrose-based solution, consisting of 205 mM sucrose, 2.5 mM KCl, 26 mM NaHCO$_3$, 1.2 mM NaH$_2$PO$_4$, 0.1 mM CaCl$_2$, 5 mM MgCl$_2$ and 10 mM D-glucose; pH set at 7.4 by gassing with carbogen (95% O$_2$-5% CO$_2$). The brain was glued upside-down and horizontal slices (400 μm thick) were cut (from 4.5 mm to 6.5 mm ventral

from bregma) in chilled sucrose-based solution, using an Integraslicer (Campden Instruments, Loughborough, UK) vibrating ceramic blade slicer. Slices from the left hippocampus, including the whole hippocampus and overlaying neocortex (Supplemental Materials 1 panel A), were immediately placed in the Haas-type interface recording chamber (kept at 32 °C), which was perfused (7 ml/min) with artificial cerebrospinal fluid (aCSF) and covered with warm, moist carbogen (0.3 l/min). The aCSF consisted of 125 mM NaCl, 3 mM KCl, 26 mM NaHCO$_3$, 1.25 mM NaH$_2$PO$_4$, 2 mM CaCl$_2$, 1 mM MgCl$_2$ and 10 mM D-glucose and was saturated with carbogen, keeping the pH at 7.4. Slices from the right hippocampus were trimmed with scalpel cuts to obtain isolated CA1 minislices, in which the CA1 cell line was kept intact, but subiculum and CA2 was kept to a minimum (Supplemental Materials 1 panel B). CA1 minislices were maintained in an interface type storage chamber, kept at 21 °C for later use.

2.3. Field potential recording of gamma oscillations

Field potentials were recorded using aCSF-filled glass pipette recording electrodes (4–5 MΩ), amplified with Neurolog NL104 AC-coupled amplifiers (Digitimer, Welwyn Garden City, UK) and band-pass filtered at 2 Hz–500 Hz with Neurolog NL125 filters (Digitimer). After main line noise (50 Hz) was eliminated with Humbug noise eliminators (Digitimer), the signal was digitized and sampled at 2 kHz using a CED-1401 (Cambridge Electronic Design, Cambridge, UK) and Spike-2 software (Cambridge Electronic Design).

Gamma (γ) oscillations were induced by carbachol (5 μM) after 60 min of rest and left to develop for 60 min. In some experiments drugs were applied to either CA1 or CA3 and diffusion from CA3 to CA1 was prevented by placing a hair covered in vacuum grease (Down Corning, Midland, USA) over CA2 (Supplemental Materials Fig. 2). A glass micropipette was filled with freshly gassed aCSF, with or without drug, at a concentration 40 times the concentration used for bath application. Addition of 0.1 mM Evans blue allowed to monitor the spread of fluid applied. The tip was broken up to the point that a minimal amount of aCSF would flow out by gravity, when touching the fluid film covering the slice. The drug was applied by a swiping movement following the cell line avoiding accumulation of fluid in one place. After 5 min the application was stopped by lifting the pipette.

2.4. Drugs

Drugs were added to the aCSF, diluted from the following stock solutions: The muscarinic acetylcholine receptor agonist carbamylcholine chloride (carbachol), 10 mM in H$_2$O; the μ–opioid receptor agonist the [D-Ala^2, NMe-Phe^4, Gly-ol^5]-enkephalin (DAMGO), 1 mM in H$_2$O; the competitive μ–opioid receptor antagonist D-Phe-Cys-Tyr-D-Trp-Arg-Thr-Pen-Thr-NH2 (CTAP), 0.2 mM in H$_2$O; the voltage-sensitive sodium channel blocker tetrodotoxin citrate (TTX), 1 mM in H$_2$O. DAMGO and CTAP were purchased from Tocris (Bristol, UK). All other drugs and aCSF salts were purchased from Sigma (Poole, UK). In control experiments equivalent vehicle (H$_2$O) applications were made.

2.5. Data analysis

Data analysis was done using Spike-2 (Cambridge Electronic Design) and MatLab (MathWorks, Natick, USA). In vitro recordings were band-pass filtered at 15–40 Hz for the slow γ band and at 40–80 Hz for the fast γ band, using a frequency-true filter with 5 Hz edge. The oscillation power was calculated over ≥60 s unfiltered recording epochs by fast Fourier transforms (1 Hz bin size, Hanning window).

To determine the relationship between oscillations recorded in CA1 and CA3, the cross-correlation and the phase-locking value (PLV) were calculated. Waveform cross-correlograms, with CA3 as reference, were calculated over 300 s epochs of band pass-filtered recordings. PLV analysis was done by a method adapted from Lachaux et al. (1999).
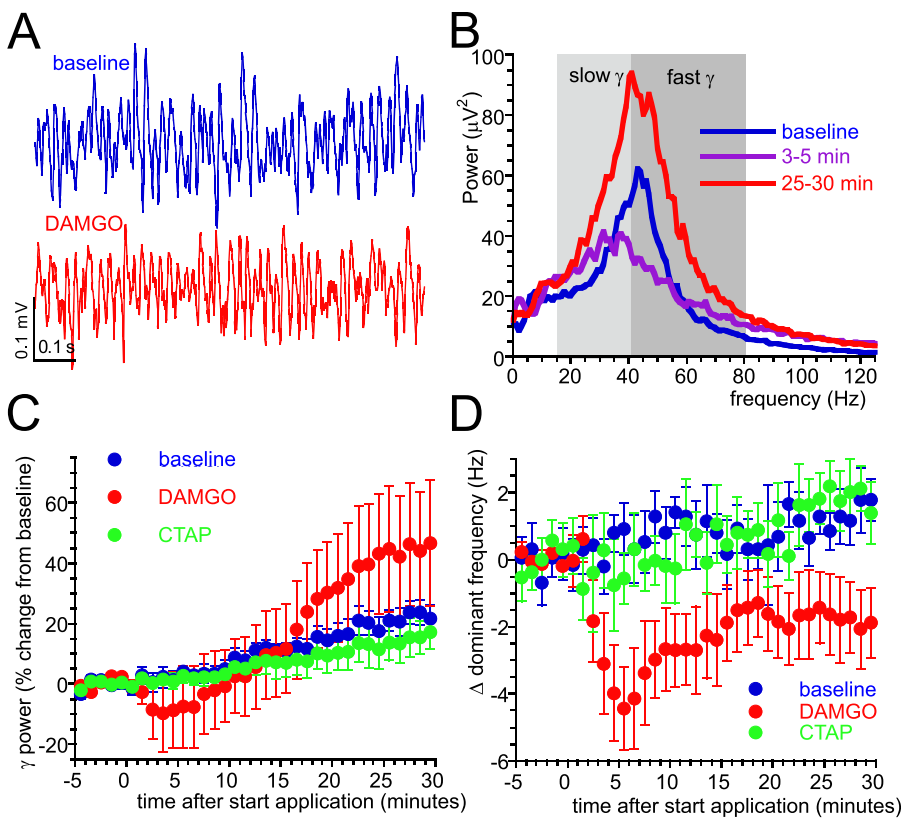
Fig. 1. MOR activation decelerates γ oscillations in CA1 minislices. **A.** Typical recordings from a CA1 minislice (see Supplemental Materials 1) show oscillatory activity before (blue trace) and after (red trace) application of the MOR agonist DAMGO (1 μM). **B.** Power spectra of the recordings in (A) before (blue line), 3–5 minutes (purple line) and 25–30 minutes (red line) after DAMGO application. Shows the biphasic nature of the effect of MOR activation on power in the γ range. **C.** The change in γ power (15–80 Hz) as function of time after application of DAMGO (n = 11, red symbols), the MOR antagonist CTAP (200 nM, n = 8, green symbols) or vehicle (n = 8, blue symbols), shows a large variability in the effect of DAMGO on γ power. Data show average and s.e.m. **D.** The change in dominant frequency as function of time after application of DAMGO, CTAP or vehicle. Details as in C. DAMGO causes a consistent early deceleration of the γ oscillation (For interpretation of the references to colour in this figure legend, the reader is referred to the web version of this article).

From band pass-filtered recordings from CA1 and CA3, a Hilbert transform provided the phase of each time point (φs) and the difference in φs between the two signals (δφs) was calculated for all time points. The phase-locking index was calculated over 10 s epochs with 5 s overlap to provide a time series of the PLV (ranging between 1: completely locked δφs and 0: completely random δφs). Event-related potentials (ERPs) were constructed by taking waveform averages of the unfiltered recording from CA1 or CA3, time-zeroed by the troughs of medium-large amplitude waves in the γ band pass-filtered recording from CA3. Care was taken to select the same size troughs before and after drug application, by setting an upper limit to the 5% largest waves at baseline and a lower limit as 50% of the upper limit.

2.6. Statistics

Data sets were found to be normally distributed and are expressed as mean ± standard error of the mean (s.e.m.). Statistical comparisons between experimental groups were made using unpaired Student's t-tests and between different conditions within one cell using paired Student's t-tests. Effects were considered significant if $P < 0.05$. Statistical analysis was done using SPSS (SPSS Inc., Chicago, USA).

3. Results

3.1. Effect of MOR modulation on γ oscillations in CA1 minislices

3.1.1. Intrinsic CA1 γ oscillation characteristics

The neuronal network in CA1, when anatomically isolated from area CA3, is known to generate its own intrinsic γ oscillation that is faster than the γ oscillation generated by the CA3 neuronal network and independent of subicular activity (Bibbig et al., 2007; Middleton et al., 2008; Pietersen, et al., 2014). Oscillatory activity was induced in CA1 minislices by adding the cholinergic receptor agonist carbachol (5 μM) to the aCSF (Pietersen et al., 2014). Recordings were made from the stratum oriens-stratum pyramidale border, where the power of intrinsic

fast γ was found to be maximal (Pietersen et al., 2014). Out of six CA1 slices placed in the recording chamber, two were selected that had developed the strongest γ oscillations (example in Fig. 1A). Taking into account the temperature dependence of gamma oscillations (Dickinson et al., 2003), we defined the γ band as 15–80 Hz, the slow γ band as 15–40 Hz and the fast γ band as 40–80 Hz. In 26 control slices the average power in the slow γ band (slow γ power) was $7.5 ± 1.2 \mu V^2$, the fast γ power was $7.0 ± 1.0 \mu V^2$ and the dominant frequency was $44.1 ± 0.7$ Hz.

3.1.2. The effect of MOR modulation on CA1 γ power and frequency

We tested the effect of the MOR agonist DAMGO and the competitive MOR antagonist CTAP on the γ oscillations in CA1 minislices, one hour after application of carbachol. All effects of drugs are expressed as changes, normalized to the five minutes before drug application (baseline) and compared to similar changes in response to vehicle application (control) that showed small, but systematic changes with time. In eight control slices, γ power (average power in the 15–80 Hz band) gradually increased by 21 ± 4% relative to baseline ($t_{(7)} = -2.98$, P = 0.020) over 30 min after vehicle application and the dominant frequency increased by 1.3 ± 0.5 Hz ($t_{(7)} = -2.41$, P = 0.047). Application of DAMGO (1 μM) did not affect γ power consistently; four slices responded with an initial suppression, followed by a later increase in γ power (example in Fig. 1B), two slices only had the early suppression and two slices only showed a power increase. Fig. 1C gives the average change in γ power, showing a biphasic effect, suggesting that the contribution of an early suppressive effect and the late enhancing effect of DAMGO differs per slice. After 30 min, γ power was 146 ± 22% of baseline ($t_{(10)} = -1.28$, P = 0.228) and not different from the change in control slices ($t_{(17)} = -0.96$, P = 0.350). However, there was a consistent reduction in the dominant frequency in the first five minutes (by −3.8 ± 1.4 Hz, $t_{(10)} = 2.70$, P = 0.022), which gradually recovered and was −1.8 ± 1.2 Hz from baseline after 30 min ($t_{(10)} = 1.64$, P = 0.131, Fig. 1D), different from the small increase in frequency observed in control slices ($t_{17} = 2.90$, P = 0.020).
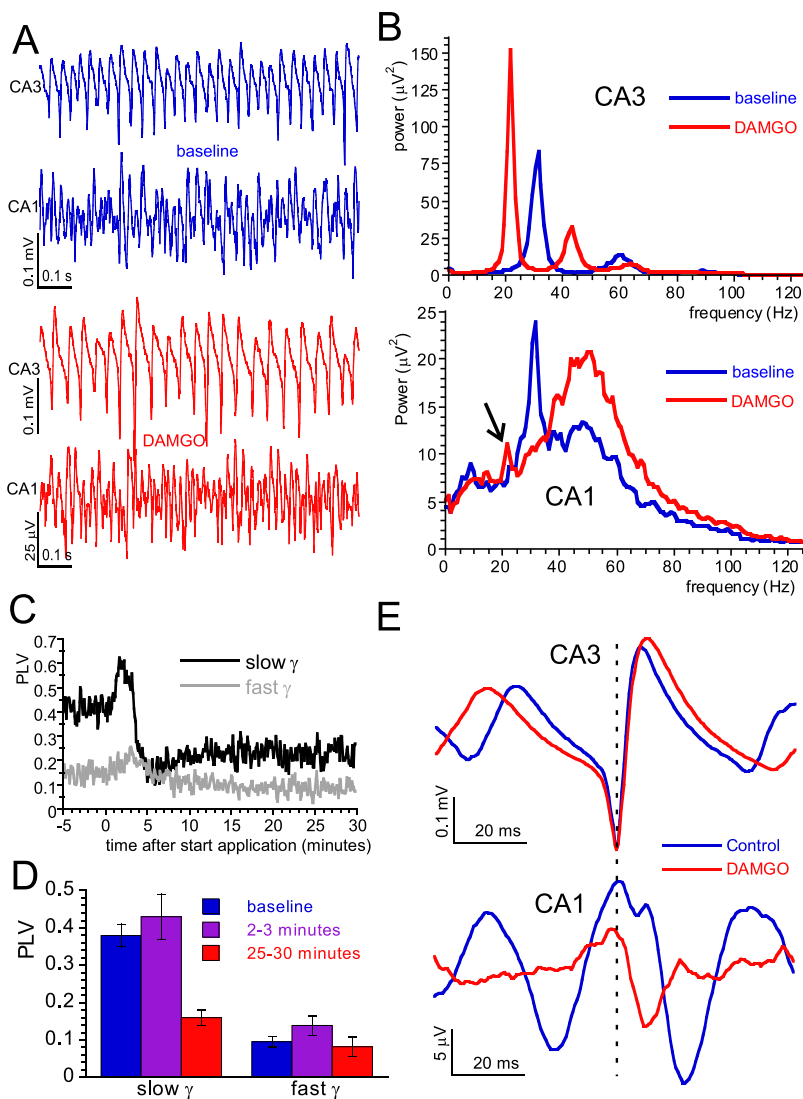
Fig. 2. MOR activation uncouples γ oscillations in CA1 from γ oscillations in CA3. A. Typical recordings from area CA3 and CA1 of an intact hippocampal slice (see Supplemental Materials 1). At baseline (blue traces) CA3 displays slow γ and CA1 a mixture of slow γ and fast γ. DAMGO application decelerates CA3 slow γ and increases the fast γ content in the CA1 recording. **B.** Power spectra of recordings in CA3 (top panel) and CA1 (bottom panel) of slice in (A) before (blue lines) and after DAMGO application (red lines). DAMGO shifts the slow γ power peak in CA3 and shifts and reduces the CA3-linked slow γ power peak in CA1 (arrow). **C.** Example of the phase-locking value (PLV) between CA3 and CA1 recordings of slice in (A), for the slow γ band (black line) and the fast γ band (grey line). DAMGO application caused a strong reduction of the slow γ PLV and a small reduction of the fast γ PLV. **D.** Histogram of the PLV for the slow γ band and fast γ band, before (blue bars), and 2–3 minutes (purple bars) and 25–30 minutes (red bars) after DAMGO application. Data are average and s.e.m. of 10 slices. **E.** ERPs in CA3 (top panel) and CA1 (bottom panel) of slice in (A), time-zeroed by the trough of medium-large-size slow γ waves in CA3 (dotted line), before (blue lines) and after DAMGO application (red lines). DAMGO reduces the slow late ERP and unmasks an earlier ERP component (For interpretation of the references to colour in this figure legend, the reader is referred to the web version of this article).

Application of CTAP (200 nM) had no effect on γ power (114 ± 4% of baseline, $t_{(7)}$ = 1.49, P = 0.181, not different from changes in control slices, $t_{(14)}$ = 0.70 P = 0.496, Fig. 1C), or on dominant frequency ($t_{(14)}$ = 1.09, P = 0.294 compared to control, Fig. 1D), suggesting that, under our experimental conditions, MORs are not activated by endogenous MOR ligands.

3.2. MOR modulation uncouples slow γ oscillations in intact hippocampal slices

3.2.1. CA1 has CA3-driven slow γ and intrinsic fast γ

Oscillatory activity was induced in intact hippocampal slices by adding carbachol (5 μM) to the aCSF. Recordings were made from CA3c stratum pyramidale and from the stratum pyramidale/stratum oriens border in CA1a, where the power of intrinsic fast γ was found to be largest (Pietersen et al., 2014). The oscillation was normally very regular in area CA3 (example in Fig. 2A) with clear power peak in the slow γ band (28.4 ± 0.3 Hz, n = 23) and second peak in the fast γ band (Fig. 2B). Because the peak frequency of the fast γ peak was always double that of the dominant frequency of the slow γ peak, and slow γ power and fast γ power covaried strongly within slices, the second peak is assumed to be the second harmonic, reflecting the saw tooth shape of the γ waveform. However, in area CA1 of the same slice the oscillation was very irregular (example in Fig. 2A) and the power spectrum often had two distinct peaks: one with a peak frequency identical to the

dominant frequency of CA3 slow γ and a shoulder or peak at higher frequencies (35–55 Hz, example in Fig. 2B). From the three slices placed in the recording chamber, the one with the largest CA1 fast γ/CA1 slow γ ratio was selected for further analysis and pharmacological experiments. The slow γ power in CA1 covaries with the CA3 slow γ power, but not with the fast γ power in CA1 (Pietersen et al., 2014), suggesting that, in part, the CA1 slow γ is driven by CA3 slow γ. If CA3 slow γ drives CA1 slow γ through Schaffer collateral-mediated inputs (Bragin et al., 1995; Fellous and Sejnowski, 2000; Fisahn et al., 1998), it is expected that the phase of the oscillation in both networks is coupled. To test this, the phase-locking value (PLV) between the CA1 signal and CA3 signal was determined. The PLV for the slow γ band was substantial (0.38 ± 0.02, n = 23), but the PLV for the fast γ band was weak (0.12 ± 0.01). In line with this, the amplitude (peak nearest to 0 ms minus following trough) of the cross-correlation between CA3 and CA1, was substantial for the slow γ band (0.78 ± 0.04), with a phase difference (time of the cross-correlation minimum) of 9.6 ± 0.4 ms, but the cross-correlation amplitude was small for the fast γ band (0.14 ± 0.02). The synchronous firing of CA3 pyramidal cells underlying CA3 slow γ, is driving slow γ in CA1 through feed-forward inhibition (Heistek et al., 2013). In order to investigate the CA3 slow γ-driven, Schaffer collateral-mediated influence on the oscillation in CA1, event-related potentials (ERPs) were constructed. Because CA3 pyramidal neurons fire close to the γ wave troughs recorded in CA3 stratum pyramidale (Fisahn et al., 1998), CA3-CA1 ERPs were

constructed using the trough of medium-large size slow γ waves in CA3 stratum pyramidale as trigger (example in Fig. 2E). These CA3-CA1 ERPs represent both Schaffer collateral-mediated excitatory post-synaptic currents (EPSCs) and feed-forward inhibitory postsynaptic currents (IPSCs). The ERP had a minimum of $28 \pm 5\,\mu V$ at $18 \pm 2\,ms$ after the population spike in CA3. These observations indicate that, in the intact slice, CA1 slow γ is, in part, phase-coupled to CA3 slow γ through Schaffer collateral inputs, whereas CA1 fast γ is mostly independent of the CA3 oscillation.

3.2.2. The effect of MOR modulation on CA3 γ power and frequency

In the mouse hippocampus slices, DAMGO reduced carbachol-induced CA3 γ power, without affecting its dominant frequency (Gulyas et al., 2010). Our prediction was to observe a similar effect in rat hippocampus slices. However, DAMGO (1 μM) did not consistently affect CA3 γ power. Seven out of ten slices had biphasic changes in CA3 slow γ power, with an early increase and later decrease, suggesting opposing effects. The remaining slices had an initial decrease followed by an increase. At 25–30 minutes after DAMGO application, CA3 slow γ was $159 \pm 28\%$ of baseline ($t_{(9)} = 1.14$, $P = 0.296$). In each slice the dominant frequency of CA3 slow γ shifted quickly, on average by $-9.7 \pm 0.4\,Hz$ ($t_{(9)} = 24.65$, $P < 0.001$).

3.2.3. The effect of MOR modulation on the CA3-driven slow γ power in CA1

In the same slices, the CA3-driven slow γ power peak in CA1 shifted to a similar frequency as in CA3, but was strongly reduced in amplitude, both in slices where DAMGO decreased CA3 slow γ power, as well as in slices where DAMGO increased CA3 slow γ power (example in Fig. 2B). To quantify this effect, the CA3 dominant frequency power (power in the range -5 Hz to $+5$ Hz from the dominant frequency in CA3) in CA1 was divided by the CA3 dominant frequency power in CA3. DAMGO reduced this CA3 dominant frequency power ratio to $37 \pm 6\%$ of that at baseline ($t_{(9)} = 6.22$, $P < 0.001$, example in Fig. 2B). This suggests that activation of MORs uncouples oscillatory activity in CA1 from the slow γ in CA3. DAMGO increased the CA1 fast γ power/CA1 slow γ power ratio by $42 \pm 11\%$ ($t_{(9)} = -3.38$, $P = 0.008$), indicating that the DAMGO-induced uncoupling of oscillatory activity in CA1 from CA3 slow γ, reduces the suppressive effect of CA3 slow γ on intrinsic fast γ in CA1, as demonstrated previously (Pietersen et al., 2014, see also Supplemental Materials 2).

3.2.4. The effect of MOR modulation on phase-coupling between CA3 γ and CA1 γ

To test the functional uncoupling of oscillatory activity in CA1 from CA3 slow γ by DAMGO, we first tested the effect of DAMGO on the PLV between the CA1 signal and the CA3 signal. In all slices where DAMGO caused an increase in CA3 slow γ power, the slow γ PLV transiently increased, to a maximum of $157 \pm 8\%$ of baseline ($t_{(6)} = -8.79$, $P < 0.001$) at 2–3 minutes after application, after which it decreased (example in Fig. 2C). In the remaining slices the slow γ PLV only decreased upon DAMGO application. Taken from its maximum value (either at baseline or after 2–3 minutes), DAMGO reduced the slow γ PLV by $70 \pm 3\%$ ($t_{(9)} = 10.46$, $P < 0.001$, Fig. 2D). In contrast DAMGO application had no consistent effect on the fast γ PLV ($83 \pm 10\%$ of baseline ($t_{(9)} = 1.65$, $P = 0.134$, Fig. 2C,D). These observations confirm that MOR activation can functionally uncouple γ in CA1 from CA3 slow γ.

3.2.5. The effect of MOR modulation on CA3-driven synaptic potentials in CA1

Because the PLV analysis does not address any DAMGO-induced change in directionality or nature of the CA3-CA1 coupling, this was assessed by cross-correlation and ERP analysis. DAMGO shifted the time of the cross-correlation minimum by $-16 \pm 4\,ms$ ($t_{(9)} = 3.84$, $P = 0.004$), suggesting that the response of the CA1 network to CA3 inputs changed in nature. In order to analyze the effect of DAMGO on the CA3-CA1 ERP, CA3 slow γ waves were selected at a fixed medium-large amplitude range, set at baseline. The CA3 waveform average of selected slow γ waves demonstrates that, despite a change in CA3 slow γ power, the trigger for the CA3-CA1 ERP in DAMGO is the same as at baseline (Fig. 2E, top panel). If MORs are selectively expressed on interneurons (Drake and Milner, 2002; Svoboda et al., 1999), the prediction is that MOR activation would reduce the feed-forward IPSC, but would not affect the EPSC. Indeed, DAMGO reduced the CA3-CA1 ERP amplitude at the time of the trough at baseline by $82 \pm 3\%$ ($t_{(9)} = -7.18$, $P < 0.001$), unmasking an earlier component (trough moved by $-11 \pm 1\,ms$, $t_{(9)} = 11.24$, $P < 0.001$) that was only visible as a notch in the waveform at baseline (example in Fig. 2E, bottom panel). The earlier component is likely to reflect the CA3-CA1 EPSC, unmasked by suppression of the subsequent feed-forward IPSC. These observations confirm that activation of MORs suppresses the feed-forward inhibition-driven slow γ in CA1, which can cause the loss of phase-coupling between CA3 slow γ and CA1 slow γ.

3.3. The effect of DAMGO is MOR-specific

To test the selectivity of MOR activation in the effect of DAMGO, we repeated the experiment in the presence of a high concentration of the competitive MOR antagonist CTAP (500 nM, applied 20 min before DAMGO). CTAP did not affect CA3 slow γ power ($116 \pm 11\%$ of baseline ($t_{(5)} = -1.53$, $P = 0.187$, example in Fig. 3C), the dominant frequency of CA3 slow γ ($0.2 \pm 0.4\,Hz$ from baseline, $t_{(5)} = 0.42$, $P = 0.695$), the CA3 dominant frequency power ratio ($91 \pm 4\%$ of baseline, $t_{(5)} = 2.07$, $P = 0.093$), the slow γ PLV ($106 \pm 3\%$ of baseline, $t_{(5)} = -1.94$, $P = 0.110$, Fig. 3B), the slow γ cross-correlation phase-difference (trough was $1.2 \pm 0.7\,ms$ from that at baseline, $t_{(5)} = -1.58$, $P = 0.180$), or the ERP amplitude at the time of the trough at baseline ($108 \pm 8\%$ of baseline, $t_{(5)} = 1.01$, $P = 0.358$, example in Fig. 3C). In the presence of CTAP, DAMGO did not affect CA3 slow γ power ($139 \pm 23\%$ of CTAP baseline, $t_{(5)} = -1.80$, $P = 0.132$), but shifted the dominant frequency of CA3 slow γ by $-2.3 \pm 0.2\,Hz$ from that at CTAP baseline ($t_{(5)} = -11.07$, $P < 0.001$, example in Fig. 3A), significantly less than the shift in the absence of CTAP ($t_{(14)} = 22.90$, $P < 0.001$). In the presence of CTAP, DAMGO did not affect the CA3 dominant frequency power ratio ($121 \pm 21\%$ of CTAP baseline, $t_{(5)} = -0.64$, $P = 0.552$), the slow γ PLV ($98 \pm 8\%$ of baseline, $t_{(5)} = 0.21$, $P = 0.840$, Fig. 3B), the slow γ cross-correlation phase-difference (trough was $1.0 \pm 0.5\,ms$ from that at CTAP baseline, $t_{(5)} = 1.94$, $P = 0.111$), or the ERP amplitude at the time of the trough at CTAP baseline ($109 \pm 4\%$ of CTAP baseline, $t_{(5)} = -1.71$, $P = 0.149$, example in Fig. 3C). Although the competitive MOR antagonist CTAP did not completely prevent the shift in CA3 slow γ dominant frequency, it prevented the phase uncoupling observed with DAMGO alone, confirming that this effect is MOR-selective.

3.4. Effect of frequency change cannot explain the uncoupling

Because the suppression of intrinsic CA1 fast γ by CA3-generated slow γ is dependent on the frequency of Schaffer collateral inputs (Pietersen et al., 2014), it is possible that the DAMGO-induced reduction of phase-coupling between CA3 slow γ and CA1 slow γ is caused by the reduced frequency of CA3 slow γ, which would allow the emergence of intrinsic CA1 fast γ. To test this, we used the benzodiazepine zolpidem that is known to reduce the frequency of CA3 slow γ by decreasing the IPSC decay rate (Heistek et al., 2013). Like the effect of DAMGO, zolpidem (1 μM) decreased the dominant frequency of CA3 slow γ in seven slices tested by $-5.5 \pm 0.6\,Hz$ ($t_{(6)} = 8.90$, $P < 0.001$) and shifted the CA3-driven slow γ power peak in CA1 by the same amount (example in Fig. 4A). Zolpidem increased CA3 slow γ power by $25 \pm 5\%$, which was not different from the change in vehicle controls ($18 \pm 2\%$, $t_{(15)} = 1.02$, $P = 0.325$). However, in contrast to the effect
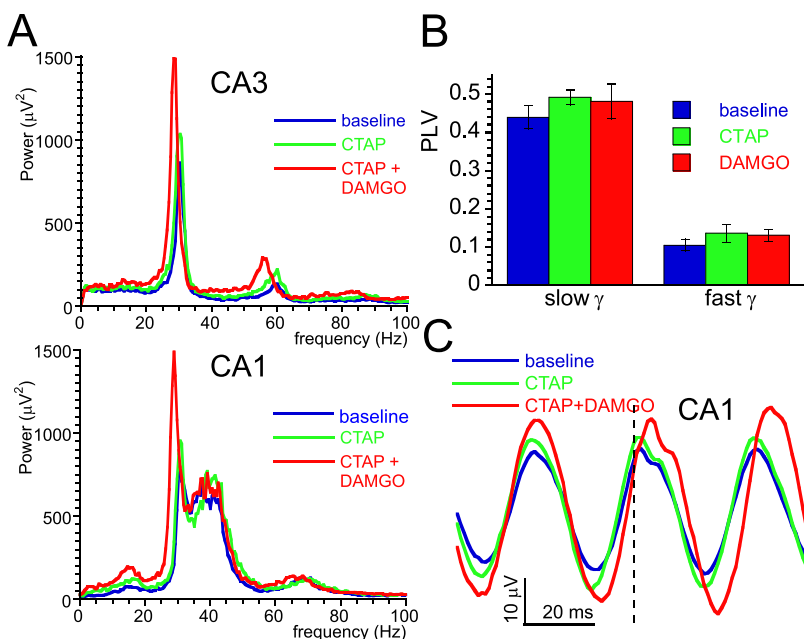
Fig. 3. DAMGO application in the presence of CTAP fails to uncouple CA1 γ from CA3 slow γ. **A.** Example of the effect of application of DAMGO (1 μM), 20 min after application of the competitive MOR antagonist CTAP (500 nM), on the power spectrum of recordings from CA3 (top panel) and CA1 (bottom panel), before (blue lines) and after CTAP application (green lines) and after addition of DAMGO (red lines). In the presence of CTAP, DAMGO does not suppress the CA3-linked slow γ power peak in CA1. **B.** Histogram of the PLV for the slow γ band and fast γ band, at baseline (blue bars), after CTAP application (green bars) and after DAMGO application (red bars). Data are average and s.e.m. of 6 slices. **C.** Example of an ERP in CA1 time-zeroed by th CA3 trough-(dotted line) at baseline, in the presence of CTAP and after DAMGO application (details as in A). In the presence of CTAP, DAMGO application did not affect the ERP. (For interpretation of the references to colour in this figure legend, the reader is referred to the web version of this article).

of DAMGO, zolpidem slightly increased the CA3 dominant frequency power in CA1 (to 122 ± 10% of baseline, $t_{(6)}$ = -1.55, P = 0.172) and increased the CA3 dominant frequency power ratio by 27 ± 4% ($t_{(6)}$ = 6.22, P < 0.001, example in Fig. 4A). Zolpidem did not affect the slow γ PLV (88 ± 8% of baseline, $t_{(6)}$ = 1.57, P < 0.177, Fig. 4B), or the slow γ cross-correlation phase difference (trough was 1.3 ± 0.6 ms from that at baseline, $t_{(6)}$ = -2.07, P = 0.084). Zolpidem reduced the CA3-CA1 ERP amplitude at the time of the trough at baseline slightly (to 78.8 ± 4.0% of baseline, $t_{(6)}$ = − 2.17, P = 0.073), significantly less than the DAMGO-induced change ($t_{(15)}$ = 7.52, P < 0.001). Zolpidem did not affect the ERP trough time (shifted by 2.1 ± 0.4 ms, $t_{(6)}$ = -2.07, P = 0.084) and waveform shape (example in Fig. 4C). These observations indicate that the DAMGO-

induced uncoupling of CA1 γ is not the result of the reduced dominant frequency of slow γ in CA3.

3.5. Local application of DAMGO identifies the effect location

3.5.1. Local application of drugs

In order to determine where in the hippocampal network DAMGO causes the uncoupling of CA1 gamma from slow γ in CA3, we applied DAMGO selectively in area CA3 or in area CA1, with the fluid film on top of the slice divided by a greased hair (Supplemental Materials 2 panel A). To ensure that the drug application would affect the entire area of interest, without spreading across the greased hair barrier, we tested the effect of TTX application (for five minutes) by a gravity fed
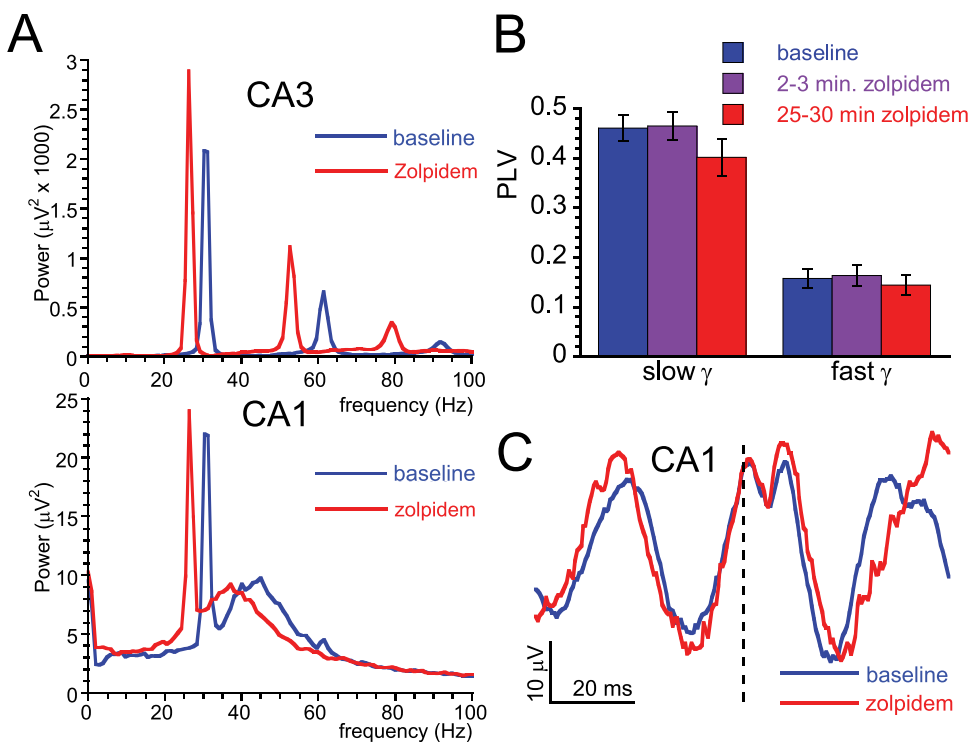

Fig. 4. Deceleration of CA3 slow γ fails to uncouple CA1 γ from CA3 slow γ. **A.** Example of the effect of zolpidem on the power spectrum of recordings from CA3 (top panel) and CA1 (bottom panel), before (blue lines) and after application of zolpidem (1 μM, red lines). Zolpidem decelerates CA3 slow γ and shifts the CA3-linked slow γ power peak in CA1, without affecting γ power in CA1. **B.** Histogram of the PLV for the slow γ band and fast γ band, before (blue bars), and 2–3 minutes (purple bars) and 25–30 minutes (red bars) after zolpidem application. Data are average and s.e.m. of 7 slices. **C.** Example of an ERP in CA1, time-zeroed by the CA3 trough-(dotted line) before (blue line) and after zolpidem application (red line). Zolpidem did not affect the ERP (For interpretation of the references to colour in this figure legend, the reader is referred to the web version of this article).
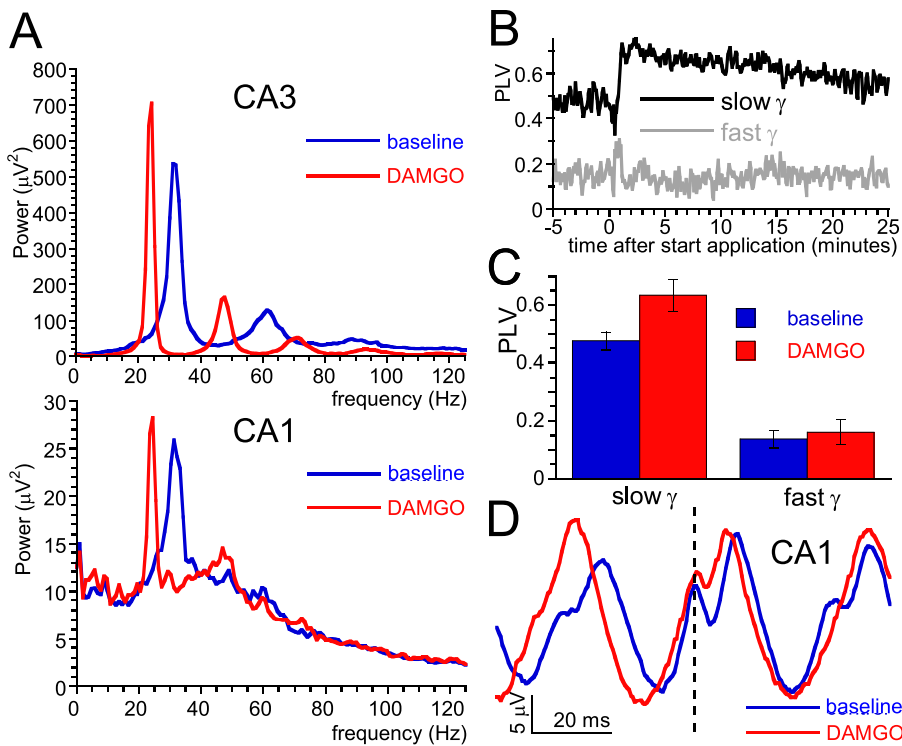
Fig. 5. DAMGO application to CA3 decelerates CA3 slow γ but fails to uncouple CA1 γ from CA3 slow γ. **A.** Example of the effect of application of DAMGO to the CA3 area only, using the greased hair as diffusion barrier, on the power spectrum of recordings from CA3 (top panel) and CA1 (bottom panel), before (blue lines) and after local application of DAMGO (red lines). DAMGO in CA3 decelerates CA3 slow γ and shifts the CA3-linked slow γ power peak in CA1, without affecting γ power in CA1. **B.** Example of the phase-locking value (PLV) between CA3 and CA1 recordings of slice in (A), for the slow γ band (black line) and the fast γ band (grey line). Data are. **C.** Histogram of the PLV for the slow γ band and fast γ band, at baseline (blue bars) and after DAMGO application to CA3 (red bars). Data are average and s.e.m. of 7 slices. **D.** Example of an ERP in CA1 time-zeroed by the CA3 trough(dotted line), before (blue line) and after DAMGO application (red line). DAMGO application to CA3 did not affect the ERP (For interpretation of the references to colour in this figure legend, the reader is referred to the web version of this article).

large-tip application pipette (Supplemental Materials 2). Application of TTX to area CA3 not only validated the method, but demonstrated, in line with our previous report (Pietersen et al., 2014), that the disappearance of the CA3 gamma-driven input to CA1 unmasked the intrinsic fast γ in CA1.

3.5.2. The effect of MOR modulation in CA3 only

Application of DAMGO (40 μM) to the entire CA3 stratum pyramidale, but avoiding CA1, decreased the dominant frequency of slow γ in CA3 by 10.6 ± 1.4 Hz ($t_{(6)} = 7.67$, P < 0.001, example in Fig. 5A), not different from the shift induced by bath application of DAMGO ($t_{(15)} = 0.72$, P = 0.485). The CA3 slow γ power increased by $49 \pm 19\%$ ($t_{(6)} = -2.49$, P = 0.047). However, in contrast to bath application of DAMGO, but similar to the effect of zolpidem, local application of DAMGO to CA3 did only shift, but not reduce the CA3 slow γ power peak in CA1 (example in Fig. 5A). DAMGO in CA3 increased the slow γ PLV (by $33 \pm 8\%$, $t_{(6)} = 4.02$, P = 0.007, Fig. 5B/C), but did not affect the CA3 dominant frequency power ratio ($106 \pm 4\%$ of baseline, $t_{(6)} = -0.33$, P = 0.751), or the slow γ cross-correlation phase difference (trough was 1.0 ± 0.6 ms from that at baseline, $t_{(6)} = 1.73$, P = 0.144). DAMGO in CA3 did not affect the CA3-CA1 ERP amplitude at the time of the trough at baseline (to $111 \pm 8\%$ of baseline, $t_{(6)} = 1.43$, P = 0.204, example in Fig. 5D). If anything, DAMGO applied to CA3 only increased the phase-coupling between CA3 and CA1 γ.

3.5.3. The effect of MOR modulation in CA1 only

Application of DAMGO to the CA1 area recorded from, while avoiding CA3 with the greased hair method, had no effect on CA3 slow γ power ($t_{(6)} = -1.66$, P = 0.148) or dominant frequency ($t_{(6)} = 0.00$, P = 0.999), but suppressed the CA3-driven slow γ power peak in CA1 (example in Fig. 6A). The CA3 dominant frequency power ratio was reduced by $56 \pm 6\%$ from that at baseline ($t_{(6)} = 4.04$, P = 0.007). DAMGO in CA1 reduced the slow γ PLV (by $-67 \pm 9\%$, $t_{(6)} = 5.82$, P = 0.001, Fig. 6B/C), but the slow γ cross correlation phase difference was not different (trough was 1.2 ± 1.4 ms from that at baseline, $t_{(6)} = 0.88$, P = 0.414). DAMGO in CA1 reduced the CA3-CA1 ERP

amplitude at the time of the trough at baseline by $54 \pm 9\%$ ($t_{(6)} = -4.99$, P = 0.002). Like with DAMGO applied to the intact slice, DAMGO in CA1 only unmasked an earlier component visible as a notch in the waveform at baseline (example in Fig. 6D). These observations indicate that MOR activation in CA1 alone is necessary and sufficient for the uncoupling of CA1 γ from slow γ in CA3, by suppression of the feed-forward IPSC, while leaving the EPSC intact.

4. Discussion

4.1. The effect of MOR activation on CA3-to-CA1 γ oscillation phase-coupling

We assessed the effect of MOR activation on the phase-locking of CA1 γ oscillations to CA3 slow γ. In CA1 minislices, MOR activation by DAMGO caused a transient reduction of the dominant frequency. When applied to the bath or locally in CA3, DAMGO did not affect CA3 γ power consistently, but strongly reduced the dominant frequency. DAMGO applied in the bath or locally in CA1, reduced the suppressive effect of CA3 slow γ on intrinsic fast γ in CA1, reduced the PLV between CA3 slow γ and CA1 slow γ, and reduced the CA3 slow γ-triggered ERP in CA1. The effects of DAMGO were prevented by the competitive MOR antagonist CTAP and could not be mimicked by reducing CA3 slow γ dominant frequency with the benzodiazepine zolpidem. These experiments suggest that, under our experimental in vitro conditions, MOR activation in CA1 is necessary and sufficient to suppress the feed-forward inhibition-driven slow γ in CA1, which can cause the loss of phase-coupling between CA3 slow γ and CA1 slow γ.

4.2. MOR activation-mediated changes in CA3 slow γ

Carbachol-induced γ oscillations in CA3 have been attributed to pyramidal-interneuron-network gamma (PING) (Fisahn et al., 1998). In the mouse hippocampus, DAMGO caused a strong suppression of carbachol-induced γ power, without an effect on dominant frequency (Gulyas et al., 2010), suggesting that PV + interneuron-mediated IPSCs, subject to suppression by MOR activation, are a sine qua non for CA3 γ
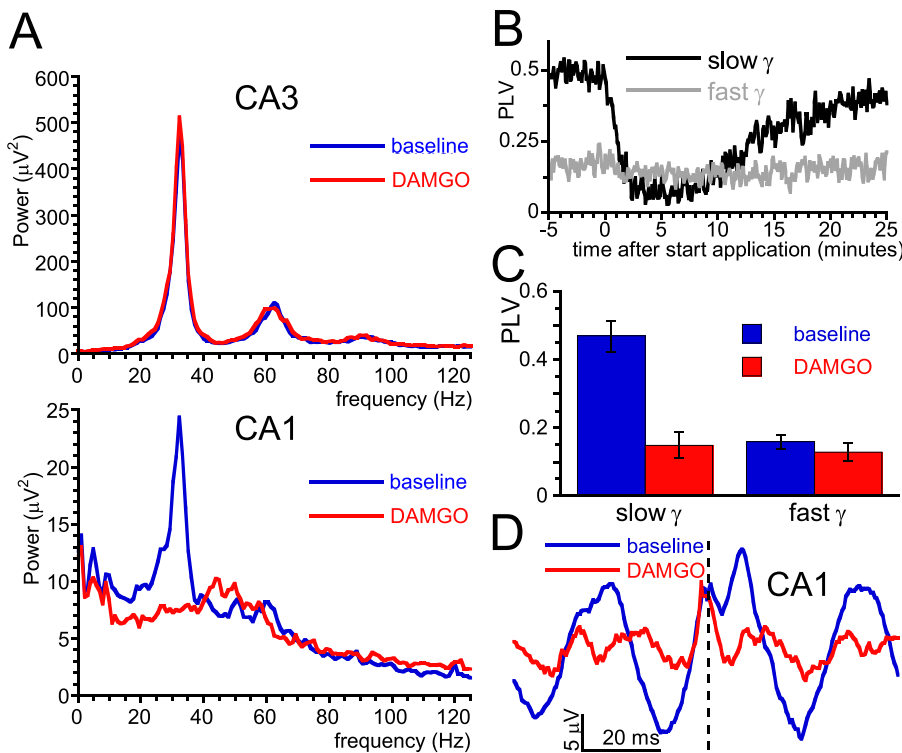
Fig. 6. DAMGO application to CA1 uncouples CA1 γ from CA3 slow γ. **A.** Example of the effect of application of DAMGO to the CA1 area only, using the greased hair as diffusion barrier, on the power spectrum of recordings from CA3 (top panel) and CA1 (bottom panel), before (blue lines) and after local application of DAMGO (red lines). DAMGO in CA1 did not affect CA3 slow γ power or dominant frequency, but reduced the CA3-linked slow γ power peak in CA1. **B.** Example of the phase-locking value (PLV) between CA3 and CA1 recordings of slice in (A), for the slow γ band (black line) and the fast γ band (grey line). DAMGO application caused a strong reduction in the slow γ PLV but had no effect on the fast γ PLV. **C.** Histogram of the PLV for the slow γ band and fast γ band, at baseline (blue bars) and after DAMGO application to CA1 (red bars). Data are average and s.e.m. of 7 slices. **D.** Example of an ERP in CA1 time-zeroed by the CA3 trough-(dotted line) before (blue line) and after DAMGO application (red line). DAMGO application to CA3 suppressed the slow late ERP and enhances an earlier, faster ERP component (For interpretation of the references to colour in this figure legend, the reader is referred to the web version of this article).

oscillations. However, in our hands, MOR activation did not affect CA3 γ power consistently, with both increases and decreases. This can be explained by inter-slice variability of the effect of MOR activation on Ivy cells (Krook-Magnuson et al., 2011). Ivy cells project perisomally and normally suppress pyramidal cell activity (Armstrong et al., 2012; Fuentealba et al., 2008a). MOR activation hyperpolarizes Ivy cells (Krook-Magnuson et al., 2011), which may increase pyramidal cell excitability and disinhibit local γ-generating networks, making the net effect of MOR activation on γ power in individual slices unpredictable. However, the DAMGO-induced strong reduction in dominant frequency was observed immediately and without exemption, suggesting significant differences between mice (Gulyas et al., 2010) and rat CA3. The deceleration of CA3 slow γ was independent of the change in γ power, suggesting that it is not related to IPSC amplitude (Atallah and Scanziani, 2009). Larger intervals are likely due to prolonged IPSCs, as this could be mimicked by the benzodiazepine zolpidem (Heistek et al., 2013), but MOR activation does not affect IPSC kinetics (Glickfeld et al., 2008). Alternatively, deceleration of γ oscillations can be caused by a reduction of tonic depolarization of interneurons, e.g. by extrasynaptic tonic GABA$_A$-ergic currents mediated by δ subunit-containing GABA$_A$ receptors expressed on interneurons (Mann and Mody, 2010; Pietersen et al., 2014). It is also possible that MOR-expressing interneurons in CA3 normally inhibit interneurons that can generate a slower PING on their own, which is unmasked by MOR activation-mediated suppression of these interneurons (Keeley et al., 2017; Middleton et al., 2008).

Because the MOR antagonist CTAP had no effect on γ power and dominant frequency in both CA3 and isolated CA1, slices contain little natural ligand for MORs under our experimental in vitro conditions.

In CA1 minislices DAMGO had similar, bi-directional effects on the intrinsic CA1 fast γ power and reduced its dominant frequency slightly. The DAMGO-induced shift to lower frequencies will lead to an underestimation of the increase in CA1 fast γ power in intact slices.

4.3. MOR activation-mediated uncoupling of CA1 slow γ from CA3 slow γ

The experiments where DAMGO was applied after the competitive

MOR antagonist CTAP, together with the local DAMGO applications, show that MOR activation in CA1 was necessary and sufficient to disrupt the phase-coupling between CA3 slow γ and CA1 slow γ. It is unlikely that this is the result of a reduced firing probability of CA3 pyramidal neurons (Middleton and McHugh, 2016), because the population spike in the CA3 waveforms selected for the CA3-CA1 ERP was identical before and after DAMGO.

CA1 slow γ emerges from synchronous feed-forward IPSCs, driven by CA3 slow γ-paced Schaffer collateral inputs (Bragin et al., 1995; Fellous and Sejnowski, 2000; Fisahn et al., 1998). The PV + interneurons involved (Bibbig et al., 2007; Tukker et al., 2007; Zemankovics et al., 2013) express MORs (Drake and Milner, 2002; Svoboda et al., 1999). MOR activation inhibits selectively feed-forward GABAergic inhibitory postsynaptic responses in CA1 pyramidal neurons (Glickfeld et al., 2008; Lupica, 1995; Masukawa and Prince, 1982), through hyperpolarization of MOR-expressing interneurons by increasing outward currents (Glickfeld et al., 2008; Svoboda et al., 1999; Wimpey and Chavkin, 1991) and through presynaptic inhibition (Capogna et al., 1993; Cohen et al., 1992; Glickfeld et al., 2008). This can explain the MOR activation-induced suppression of phase-coupling between CA3 slow γ and CA1 slow γ. Given the slow IPSC kinetics of MOR-expressing Ivy cells (Fuentealba et al., 2008a), modulating their activity by MOR activation is unlikely to affect the γ phase-coupling (Armstrong et al., 2012). Because the suppression of intrinsic CA1 fast γ by CA3 slow γ reduced with the frequency of Schaffer collateral inputs (Pietersen et al., 2014), the loss of phase-coupling could alternatively be caused by the DAMGO-induced deceleration of CA3 slow γ. However, the deceleration of CA3 slow γ by zolpidem or local application of DAMGO to CA3, did not affect the phase-coupling. Furthermore when DAMGO was applied to CA1 only the phase-coupling reduced without deceleration of CA3 slow γ.

4.4. MOR activation-mediated facilitation of intrinsic CA1 fast γ

DAMGO application increased CA1 fast γ power in slices with clear intrinsic CA1 fast γ and unmasked intrinsic CA1 fast γ in slices with mainly CA3-driven CA1 slow γ. The effect of MOR activation in CA1

was similar to lesioning Schaffer collaterals (Pietersen et al., 2014) or inactivating CA3 with TTX (Supplemental materials 2, panel C), whereas low-intensity Schaffer collateral stimulation at slow γ frequencies, suppresses intrinsic CA1 fast γ (Pietersen et al., 2014). Since intrinsic CA1 fast γ is at least partly PING, dependent on pyramidal neuron firing (Pietersen et al., 2014), this suggests that in intact slices the intrinsic CA1 PING is suppressed by CA3 slow γ-driven feed-forward MOR-expressing interneuron activity. CA1 pyramidal cell excitability is suppressed by feed-forward activation of basket cells (Bibbig et al., 2007; Csicsvari et al., 2003) and Ivy cells (Fuentealba et al., 2008a; Armstrong et al., 2012) amongst others. When rescued from this phasic and/or tonic suppression by MOR activation, intrinsic fast PING can emerge in the disinhibited CA1 network (Pietersen et al., 2014; Zemankovics et al., 2013).

In addition, two interneuron populations that differ in IPSC decay rate and mutually inhibit each other, can give rise to fast γ and slow γ alternating within the same area (Keeley et al., 2017; Middleton et al., 2008). Similarly, an increased activity of an interneuron population with a faster IPSC decay rate (Heistek et al., 2010) may contribute to the emergence of intrinsic CA1 fast γ in the presence of DAMGO.

4.5. Routing of information to CA1 by the θ phase

During active behaviors, like exploration and object recognition, CA1 slow γ and fast γ are prominent on different θ cycles and at different θ phases (Colgin et al., 2009; Schomburg et al., 2014). It is possible that the θ input from the medial septum mediates the switch between slow γ and fast γ, by varying the activity of feed-forward interneurons, which would vary the firing probability of CA1 pyramidal cells and, with it, the strength of intrinsic CA1 fast γ. This could be achieved by modulation of the strength of their excitatory inputs from CA3 (Middleton and McHugh, 2016) and/or by modulation of their excitability. Interneuron excitability is under control by GABAergic inputs from the medial septum, but this is not selective for feed-forward interneurons (Toth et al., 1997; Wulff et al., 2009). A more feed-forward interneuron-specific θ-linked modulation could arise from the θ phase-modulated activity of enkephalin-expressing interneurons that target PV + interneurons (Blasco-Ibanez et al., 1998; Fuentealba et al., 2008b) and release enkephalin upon burst firing induced by θ phased inputs (Fuentealba et al., 2008b). When MOR activation suppresses the CA3-CA1 phase-locking, the intrinsic CA1 fast γ can phase-lock with the fast γ in the MEC (Schomburg et al., 2014).

The θ phased routing of information from CA3 or MEC (Colgin et al., 2009; Schomburg et al., 2014) has been linked to the encoding and retrieval of episodic and spatial memories (Hasselmo, 2005; Jensen and Lisman, 2005) as it allows for segregation of information steams involved in encoding and recall of memory traces (Bieri et al., 2014; Colgin, 2015). It is therefore possible that the morphine-induced impairment of memory retrieval (Ghasemzadeh and Rezayof, 2016; Meilandt et al., 2004) is caused by a constant MOR activation that will disrupt the CA3 to CA1 phase-locking and segregation of information streams. This hypothesis should be assessed by testing the effect of selective MOR agonists on the θ modulation of CA1 γ oscillations and information routing.

5. Conclusions

MOR activation reduces the dominant frequency of CA3 slow γ and CA1 intrinsic fast γ, without consistent effect on γ power.

MOR activation in CA1 is sufficient and necessary to disrupt the phase-coupling between CA3 slow γ and CA1 slow γ.

The disruption is not caused by the reduction in dominant frequency of CA3 slow γ.

MOR-expressing CA1 interneurons, feed-forwardly activated by Schaffer collaterals, are likely to be responsible for the phase-coupling between CA3 and CA1 in vitro.

Theta-phased opioid release may dynamically modulate the routing of information between CA3-to-CA1 and MEC-to-CA1.

Conflict of interest

The authors have no competing interests to declare

Compliance with ethical standards

All procedures conformed to the UK Animals (Scientific Procedures) Act 1986 and were approved by the Biomedical Ethics Review Sub-committee of the University of Birmingham and by the Animal ethics and administrative council of Henan province, P.R. China. All efforts were made to minimize animal suffering and to reduce the number of animals used.

Contribution disclosure

MV designed the study, SA, GN and YZ did the experiments, YZ, YW and MV wrote and discussed the paper. All authors have approved the final article

Appendix A. Supplementary data

Supplementary data associated with this article can be found, in the online version, at https://doi.org/10.1016/j.ibror.2019.01.004.

References

Armstrong, C., Krook-Magnusson, E., Soltez, I., 2012. Neurogliaform and Ivy cells: a major family of nNOS expressing GABAergic neurons. Front. Neural Circuits 6, 23. https://doi.org/10.3389/fncir.2012.00023.

Atallah, B.V., Scanziani, M., 2009. Instantaneous modulation of gamma oscillation frequency by balancing excitation with inhibition. Neuron 62, 566–577.

Belluscio, M.A., Mizuseki, K., Schmidt, R., Kempter, R., Buzsaki, G., 2012. Cross-frequency phase-phase coupling between theta and gamma oscillations in the hippocampus. J. Neurosci. 32, 423–435.

Bibbig, A., Middleton, S., Racca, C., Gillies, M.J., Garner, H., LeBeau, F.E., Davies, C.H., Whittington, M.A., 2007. Beta rhythms (15-20 hz) generated by nonreciprocal communication in hippocampus. J. Neurophysiol. 97, 2812–2823.

Bieri, K.W., Bobbitt, K.N., Colgin, L.L., 2014. Slow and fast gamma rhythms coordinate different spatial coding modes in hippocampal place cells. Neuron 82, 670–681.

Blasco-Ibanez, J.M., Martinez-Guijarro, F.J., Freund, T.F., 1998. Enkephalin-containing interneurons are specialized to innervate other interneurons in the hippocampal CA1 region of the rat and guinea-pig. Eur. J. Neurosci. 10, 1784–1795.

Bragin, A., Jandó, G., Nádasdy, Z., Hetke, J., Wise, K., Buzsáki, G., 1995. Gamma (40-100 hz) oscillation in the hippocampus of the behaving rat. J. Neurosci. 15, 47–60.

Buzsáki, G., Buhl, D.L., Harris, K.D., Csicsvari, J., Czeh, B., Morozov, A., 2003. Hippocampal network patterns of activity in the mouse. Neuroscience 116, 201–211.

Capogna, M., Gähwiler, B.H., Thompson, S.M., 1993. Mechanism of μ-opioid receptor-mediated presynaptic inhibition in the rat hippocampus in vitro. J. Physiol. (Lond.) 470, 539–558.

Cohen, G.A., Doze, V.A., Madison, D.V., 1992. Opioid inhibition of GABA release from presynaptic terminals of rat hippocampal interneurons. Neuron 9, 325–335.

Colgin, L.L., 2015. Do slow and fast gamma rhythms correspond to distinct functional states in the hippocampal network? Brain Res. 1621, 309–315.

Colgin, L.L., Moser, E.I., 2010. Gamma oscillations in the hippocampus. Physiology (Bethesda) 25, 319–329.

Colgin, L.L., Denninger, T., Fyhn, M., Hafting, T., Bonnevie, T., Jensen, O., Moser, M.B., Moser, E.I., 2009. Frequency of gamma oscillations routes flow of information in the hippocampus. Nature 462, 353–357.

Csicsvari, J., Jamieson, B., Wise, K.D., Buzsáki, G., 2003. Mechanisms of gamma oscillations in the hippocampus of the behaving rat. Neuron 37, 311–322.

Dickinson, R., Awaiz, S., Whittington, M.A., Lieb, W.R., Franks, N.P., 2003. The effects of general anaesthetics on carbachol-evoked gamma oscillations in the rat hippocampus in vitro. Neuropharmacol. 44, 864–872.

Drake, C.T., Milner, T.A., 2002. Mu opioid receptors are in discrete hippocampal inter-neuron subpopulations. Hippocampus 12, 119–136.

Fellous, J.-M., Sejnowski, T.J., 2000. Cholinergic induction of oscillations in the hippocampal slice in the slow (0.5-2 Hz), theta (5-12 hz) and gamma (35-70 Hz) bands. Hippocampus 10, 187–197.

Fisahn, A., Pike, F.G., Buhl, E.H., Paulsen, O., 1998. Cholinergic induction of network oscillations at 40 Hz in the hippocampus in vitro. Nature 394, 186–189.

Fries, P., 2009. Neuronal gamma-band synchronization as a fundamental process in cortical computation. Annu. Rev. Neurosci. 32, 209–224.

Fuentealba, P., Begum, R., Capogna, M., Jinno, S., Marton, L.F., Csicsvari, J., Thomson, A., Somogyi, P., Klausberger, T., 2008a. Ivy cells: a population of nitric-oxide-producing, slow-spiking GABAergic neurons and their involvement in hippocampal network activity. Neuron 57, 917–929.

Fuentealba, P., Tomioka, R., Dalezios, Y., Marton, L.F., Studer, M., Rockland, K., Klausberger, T., Somogyi, P., 2008b. Rhythmically active enkephalin-expressing gabaergic cells in the CA1 area of the hippocampus project to the subiculum and preferentially innervate interneurons. J. Neurosci. 28, 10017–10022.

Ghasemzadeh, Z., Rezayof, A., 2016. Role of hippocampal and prefrontal cortical signaling pathways in dextromethorphan effect on morphine-induced memory impairment in rats. Neurobiol. Learn. Mem. 128, 23–32.

Glickfeld, L.L., Atallah, B.V., Scanziani, M., 2008. Complementary modulation of somatic inhibition by opioids and cannabinoids. J. Neurosci. 28, 1824–1832.

Gulyas, A.I., Szabo, G.G., Ulbert, I., Holderith, N., Monyer, H., Erdelyi, F., Szabo, G., Freund, T.F., Hajos, N., 2010. Parvalbumin-containing fast-spiking basket cells generate the field potential oscillations induced by cholinergic receptor activation in the hippocampus. J. Neurosci. 30, 15134–15145.

Hasselmo, M.E., 2005. What is the function of hippocampal theta rhythm?–linking behavioral data to phasic properties of field potential and unit recording data. Hippocampus 15, 936–949.

Heistek, T.S., Timmerman, A.J., Spijker, S., Brussaard, A.B., Mansvelder, H.D., 2010. GABAergic synapse properties may explain genetic variation in hippocampal network oscillations in mice. Front. Cell. Neurosci. 4, 18. https://doi.org/10.3389/fncel.2010.00018.

Heistek, T.S., Ruiperez-Alonso, M., Timmerman, A.J., Brussaard, A.B., Mansvelder, H.D., 2013. Alpha2-containing GABA$_A$ receptors expressed in hippocampal region CA3 control fast network oscillations. J. Physiol. 591, 845–858.

Jensen, O., Lisman, J.E., 2005. Hippocampal sequence-encoding driven by a cortical multi-item working memory buffer. Trends Neurosci. 28, 67–72.

Keeley, S., Fenton, A.A., Rinzel, J., 2017. Modeling fast and slow gamma oscillations with interneurons of different subtype. J. Neurophysiol. 117, 950–965.

Krook-Magnuson, E., Luu, L., Lee, S.H., Varga, C., Soltesz, I., 2011. Ivy and neurogliaform interneurons are a major target of mu-opioid receptor modulation. J. Neurosci. 31, 14861–14870.

Lachaux, J.P., Rodrigues, E., Martinerie, J., Varela, J.P., 1999. Measuring phase synchrony in brain signals. Hum. Brain Mapp. 8, 194–208.

Lupica, C.R., 1995. Delta and mu enkephalins inhibit spontaneous GABA-mediated IPSCs via a cyclic amp-independent mechanism in the rat hippocampus. J. Neurosci. 15, 737–749.

Mann, E.O., Mody, I., 2010. Control of hippocampal gamma oscillation frequency by tonic inhibition and excitation of interneurons. Nat. Neurosci. 13, 205–212.

Masukawa, L.M., Prince, D.A., 1982. Enkephalin inhibition of inhibitory input to CA1 and CA3 pyramidal neurons in the hippocampus. Brain Res. 249, 271–280.

Meilandt, W.J., Barea-Rodriguez, E., Harvey, S.A., Martinez, J.L.Jr., 2004. Role of hippocampal CA3 mu-opioid receptors in spatial learning and memory. J. Neurosci. 24, 2953–2962.

Middleton, S.J., McHugh, T.J., 2016. Silencing CA3 disrupts temporal coding in the CA1 ensemble. Nat. Neurosci. 19, 945–951.

Middleton, S., Jalics, J., Kispersky, T., LeBeau, F.E., Roopun, A.K., Kopell, N.J., Whittington, M.A., Cunningham, M.O., 2008. NMDA receptor-dependent switching between different gamma rhythm-generating microcircuits in entorhinal cortex. Proc. Natl. Acad. Sci. U. S. A. 105, 18572–18577.

Montgomery, S.M., Buzsaki, G., 2007. Gamma oscillations dynamically couple hippocampal CA3 and CA1 regions during memory task performance. Proc. Natl. Acad. Sci. U. S. A. 104, 14495–14500.

Pietersen, A.N., Ward, P.D., Hagger-Vaughan, N., Wiggins, J., Jefferys, J.G., Vreugdenhil, M., 2014. Transition between fast and slow gamma modes in rat hippocampus area CA1 in vitro is modulated by slow CA3 gamma oscillations. J. Physiol. (Paris) 592, 605–620.

Price, C.J., Cauli, B., Kovacs, E.R., Kulik, A., Lambolez, B., Shigemoto, R., Capogna, M., 2005. Neurogliaform neurons form a novel inhibitory network in the hippocampal CA1 area. J. Neurosci. 25, 6775–6786.

Schomburg, E.W., Fernandez-Ruiz, A., Mizuseki, K., Berenyi, A., Anastassiou, C.A., Koch, C., Buzsaki, G., 2014. Theta phase segregation of input-specific gamma patterns in entorhinal-hippocampal networks. Neuron 84, 470–485.

Senior, T.J., Huxter, J.R., Allen, K., O'Neill, J., Csicsvari, J., 2008. Gamma oscillatory firing reveals distinct populations of pyramidal cells in the CA1 region of the hippocampus. J. Neurosci. 28, 2274–2286.

Svoboda, K.R., Adams, C.E., Lupica, C.R., 1999. Opioid receptor subtype expression defines morphologically distinct classes of hippocampal interneurons. J. Neurosci. 19, 85–95.

Toth, K., Freund, T.F., Miles, R., 1997. Disinhibition of rat hippocampal pyramidal cells by GABAergic afferents from the septum. J. Physiol. 500, 463–474.

Tukker, J.J., Fuentealba, P., Hartwich, K., Somogyi, P., Klausberger, T., 2007. Cell type-specific tuning of hippocampal interneuron firing during gamma oscillations in vivo. J. Neurosci. 27, 8184–8189.

Wimpey, T.L., Chavkin, C., 1991. Opioids activate both an inward rectifier and a novel voltage-gated potassium conductance in the hippocampal formation. Neuron 6, 281–289.

Wulff, P., Ponomarenko, A.A., Bartos, M., Korotkova, T.M., Fuchs, E.C., Bahner, F., Both, M., Tort, A.B., Kopell, N.J., Wisden, W., Monyer, H., 2009. Hippocampal theta rhythm and its coupling with gamma oscillations require fast inhibition onto parvalbumin-positive interneurons. Proc. Natl. Acad. Sci. U. S. A. 106, 3561–3566.

Zemankovics, R., Veres, J.M., Oren, I., Hajos, N., 2013. Feedforward inhibition underlies the propagation of cholinergically induced gamma oscillations from hippocampal CA3 to CA1. J. Neurosci. 33, 12337–12351.